

Possibility of n-type doping in CaAl_2Si_2 -type Zintl phase compound CaZn_2X_2 ($X = \text{As}, \text{P}$)

Kazutaka Nishiguchi,¹ Masayuki Ochi,¹ Chul-Ho Lee,² and Kazuhiko Kuroki¹

¹*Department of Physics, Osaka University, 1-1 Machikaneyama-cho, Toyonaka, Osaka 560-0043, Japan*

²*National Institute of Advanced Industrial Science and Technology (AIST), Tsukuba, Ibaraki 305-8568, Japan*

(Dated: September 24, 2021)

Motivated by a recent theoretical suggestion that doping electrons into various CaAl_2Si_2 -type Zintl phase compounds may give rise to high thermoelectric performance, we explore the possibility of n-type (electron carrier) doping of CaZn_2X_2 ($X = \text{As}, \text{P}$) using first principles calculation. We consider n-type doping of CaZn_2X_2 with the following two situations: interstitial-site doping of alkaline earth metals AE ($= \text{Mg}, \text{Ca}, \text{Sr}, \text{Ba}$) and group 3 elements $G3$ ($= \text{Sc}, \text{Y}, \text{La}$), and $G3$ substitutional doping for the Ca site. The evaluation of the formation energy of these defects in various charged states reveals that the interstitial-site doping of $AE = \text{Ca}/\text{Mg}$ or $G3 = \text{Sc}/\text{Y}$, and $G3 = \text{La}/\text{Y}$ substitutional doping for the Ca site are relatively favorable among the possibilities considered. In particular, the formation energy of the La substitutional doping for the Ca site is the lowest among the considered cases both for CaZn_2X_2 ($X = \text{As}, \text{P}$) and is negative, which implies that La is expected to be substituted for the Ca site and provide electron carriers spontaneously. We also find that for each doping case considered, the formation energy of the defects is smaller for $X = \text{As}$ than for $X = \text{P}$, which suggests that former is relatively easier to realize n-type doping than the latter.

I. INTRODUCTION

Thermoelectric devices enable us to directly convert waste heat into electric current, so that not only thermoelectric (Seebeck) effect is one of the most fundamental and intriguing quantum mechanical phenomena in condensed matter physics, but also thermoelectric materials are important applications in terms of clean and sustainable energy.^{1,2} Conversion efficiency of thermoelectric generators is evaluated by the dimensionless figure of merit $ZT = \sigma S^2 T / \kappa$ and power factor $PF = \sigma S^2$, where σ is the electrical conductivity, S is the Seebeck coefficient, κ is the thermal conductivity, and T is the absolute temperature. The thermal conductivity can be usually divided into the lattice and carrier contributions ($\kappa = \kappa_{\text{lat}} + \kappa_{\text{el}}$), so that the phonon structures as well as the electronic structures play an important role for thermoelectric performance.

A simple strategy to achieve high thermoelectric efficiency is to realize both of large power factor and small thermal conductivity at the same time. Nanostructuring can suppress the lattice thermal conductivity κ_{lat} while keeping high carrier mobility.³⁻⁵ On the other hand, it is in general difficult to enhance PF because σ and S are difficult to increase simultaneously due to the trade-off relation between them against the carrier concentration.

In terms of electronic band structures, high group velocity of electrons and large density of states (DOS) around the Fermi level enable us to enhance PF . There have been several theoretical proposals for specific band structures that can give rise to large power factor: multi-valley⁶, pudding-mold-type⁷, and low dimensional band structures.⁸⁻¹⁰ Especially, multi-valley band structures are suitable for designing high performance thermoelectric materials, where chemical doping and substitution enable us to control the valley degeneracy through the change in the electronic and crystal structure. In fact, high performance thermoelectric materials $\alpha\text{-MgAgSb}$ ($ZT = 1.2\text{--}1.4$ at 550 K)¹¹ and $\text{Mg}_{3+\delta}(\text{Sb}, \text{Bi}, \text{Te})_2$ ($ZT = 1.5$ at 716 K)¹²⁻¹⁴ are known to be good examples that have multi-valley band structures.

In recent years, Zintl phase compounds have attracted

much interest both experimentally and theoretically as high performance thermoelectric materials.^{12,15-18} Among them, $\text{Yb}(\text{Cd}, \text{Zn})_2\text{Sb}_2$ ¹⁸ and $\text{Mg}_{3+\delta}(\text{Sb}, \text{Bi}, \text{Te})_2$ ¹²⁻¹⁴ have large $ZT > 1$, and they are 122 Zintl phase compounds AB_2X_2 , whose A is alkaline earth metal or lanthanoid, B is Mg, Zn, or Cd, and X is pnictogen. 122 Zintl phase compounds have CaAl_2Si_2 -, BaCu_2S_2 -, or ThCr_2Si_2 -type crystal structure,¹⁹ and especially the CaZn_2Si_2 -type structure with the $P\bar{3}m1$ space group often exhibits large $ZT > 1$ in both the n-type and p-type compounds. It is understood that high thermoelectric performance of the CaZn_2Si_2 -type compounds can be caused by the multi-valley band structure.²⁰⁻²²

Very recently, thermoelectric performance of many kinds of CaAl_2Si_2 -type Zintl phase compounds has been theoretically estimated by first-principles band calculations.²³ This work suggests that CaZn_2X_2 ($X = \text{Sb}, \text{As}, \text{P}$) gives large ZT in the electron-doped regime due to its high valley degeneracy of the electronic band structure. Indeed, this kind of the 122 Zintl phase compounds have been synthesized²⁴⁻²⁶ and their electronic structure have also been investigated theoretically.^{22,27} However, these 122 Zintl phase compounds become p-type semiconductors because the cation-site vacancies are easily formed under usual synthesis conditions.^{12,13,19,28} Considering that high-performance thermoelectric material $\text{Mg}_{3+\delta}(\text{Sb}, \text{Bi}, \text{Te})_2$ was successfully realized by n-type doping,¹²⁻¹⁴ it is worth investigating whether it is possible to introduce electron carriers into CaZn_2X_2 .

Motivated by the above background, we explore the possibility of n-type doping of CaAl_2Si_2 -type Zintl phase compounds CaZn_2X_2 ($X = \text{As}, \text{P}$) using first-principle calculations based on the density functional theory (DFT). The possibility of n-type (electron carrier) doping into CaZn_2X_2 is considered with the following two situations: interstitial-site doping of the alkaline earth metals AE ($= \text{Mg}, \text{Ca}, \text{Sr}, \text{Ba}$) and group 3 elements $G3$ ($= \text{Sc}, \text{Y}, \text{La}$), and $G3$ substitutional doping for the Ca site. To see this, the formation energy of the chemical doping is evaluated numerically with the supercell approach. We can find that the interstitial-site doping of $AE = \text{Ca}, \text{Mg}$ or $G3 = \text{Sc}, \text{Y}$, and $G3 = \text{La}, \text{Y}$ substitutional doping for the

Ca site is favorable both for CaZn_2X_2 ($X = \text{As}, \text{P}$) in terms of energy stability. In particular, the formation energy of the La substitutional doping for the Ca site is the lowest among the considered cases both for CaZn_2X_2 ($X = \text{As}, \text{P}$) and is negative so that La is expected to be substituted for the Ca site and provide electron carriers spontaneously. We can also see that each formation energy for CaZn_2As_2 is smaller than that for CaZn_2P_2 as a whole, so that n-type doping is considered to be relatively easier in CaZn_2As_2 than in CaZn_2P_2 .

II. METHOD

A. Theory and Model

In order to describe dopants and defects in a crystal under periodic boundary conditions, the supercell approach is adopted in the DFT calculations: we numerically investigate $N_1 \times N_2 \times N_3$ ($N_{1,2,3} \in \mathbb{N}$) supercells whose supercell lattice vectors are $\mathbf{A}_i = N_i \mathbf{a}_i$ ($i = 1, 2, 3$) with \mathbf{a}_i being the i -th primitive lattice vector. In this study, the atomic positions in the supercell are relaxed in the structural optimization after the lattice constants and atomic positions of the primitive cell are optimized. To consider the possibility of chemical doping, the dopant/defect formation energy of charged states is calculated using the supercells. The formation energy can be obtained from the supercell calculations,^{29,30} as

$$E_{\text{form}}[D^q] = \{E[D^q] + E^{\text{corr}}[D^q]\} - E_{\text{P}} - \sum_i n_i \mu_i + qE_{\text{F}}, \quad (1)$$

where $E[D^q]$ and E_{P} denote the total energy of the supercell with dopant D^q in charged state q and that of the perfect crystal supercell without any dopants and defects, respectively. $E^{\text{corr}}[D^q]$ represents its image-charge correction as discussed below. Also, n_i represents the number of removed or added atom i with the chemical potential μ_i , and E_{F} is the Fermi level, i.e., the chemical potential of the charge reservoir.

Since the periodicity of systems under periodic boundary conditions is an inevitable artifact in the supercell approach, we evaluate the formation energy in the dilute limit by including the energy correction of the finite size effects. For a cubic (isotropic) supercell, the image-charge correction in charged state q , $E_{\text{iso}}^{\text{corr}}$, can be written as a function of the linear dimension of the supercell L ,

$$E_{\text{iso}}^{\text{corr}} = \frac{q^2 \alpha}{2\epsilon L} - \frac{2\pi q Q}{3\epsilon L^3} + \frac{2\pi p^2}{3\epsilon L^3} + O(L^{-5}). \quad (2)$$

Furthermore, α , ϵ , p , and Q represents the Madelung constant, dielectric constant, and dipole and quadrupole moment of the system.³¹⁻³⁴ Note that here the dielectric constant ϵ is a scalar quantity since the expression in Eq. (2) is the result for cubic (isotropic) systems. This quantity should be treated as a dielectric tensor $\hat{\epsilon}$ when one considers anisotropic systems like the 122 Zintl phase compound CaZn_2X_2 ($X = \text{As}, \text{P}$) in this study. In particular, the counterpart of the second term in Eq. (2), namely, the point-charge correction $q^2 \alpha / 2\epsilon L$, for

anisotropic systems can be given as³⁵⁻³⁷

$$E_{1/L}^{\text{corr}} = -\frac{q^2}{2} \left[\sum_{\mathbf{R}_i \neq \mathbf{0}} \frac{1}{\sqrt{\det \hat{\epsilon}}} \frac{\text{erfc}(\eta \sqrt{\mathbf{R}_i \cdot \hat{\epsilon}^{-1} \cdot \mathbf{R}_i})}{\sqrt{\mathbf{R}_i \cdot \hat{\epsilon}^{-1} \cdot \mathbf{R}_i}} + \frac{4\pi}{\Omega} \sum_{\mathbf{G}_i \neq \mathbf{0}} \frac{\exp(-\mathbf{G}_i \cdot \hat{\epsilon} \cdot \mathbf{G}_i / 4\eta^2)}{\mathbf{G}_i \cdot \hat{\epsilon} \cdot \mathbf{G}_i} - \frac{2\eta}{\sqrt{\pi \det \hat{\epsilon}}} - \frac{\pi}{\eta^2 \Omega} \right], \quad (3)$$

where the sum over \mathbf{R}_i (\mathbf{G}_i) extends over all vectors of the supercell direct (reciprocal) lattice except for \mathbf{R}_i (\mathbf{G}_i) = $\mathbf{0}$, $\Omega = |\mathbf{A}_1 \cdot (\mathbf{A}_2 \times \mathbf{A}_3)| = N_1 N_2 N_3 V$ denotes the supercell volume with $V = |\mathbf{a}_1 \cdot (\mathbf{a}_2 \times \mathbf{a}_3)|$ being the primitive cell volume, and η is a suitably chosen convergence factor ($\sim \min\{|\mathbf{G}_i|\}$).

In this study, the formation energy in the dilute limit is evaluated by extrapolating the numerical results of the supercell calculations as a function of the linear dimension of the supercell $L = \sqrt[3]{\Omega}$, where the point-charge correction $E_{1/L}^{\text{corr}}$ is taken into account. $E_{1/L}^{\text{corr}}$ can be obtained from the macroscopic static dielectric tensor $\hat{\epsilon}$ through Eq. (3). The macroscopic static dielectric tensor including the ionic contribution is calculated based on the density functional perturbation theory, where the local field effect with respect to the Hartree and the exchange-correlation potential is included. The derivative of the cell-periodic part of the Kohn-Sham orbitals are calculated using the finite-difference method.

B. Numerical Methods

To numerically evaluate the formation energy of chemical doping in CaZn_2X_2 , first-principles calculations based on DFT are performed within the generalized gradient approximation (GGA). We perform spin-polarized DFT calculations with the Perdew–Burke–Ernzerhof (PBE) exchange-correlation functional³⁸ and the projector augmented wave (PAW) method.^{39,40} In the PAW potentials, core-electron orbitals are set for each element as Ca:[Ne], Zn:[Ar], As:[Ar]3d¹⁰, P:[Ne], Mg:[He], Sr:[Ar]3d¹⁰, Ba:[Kr]4d¹⁰, Sc:[Ne], Y:[Ar]3d¹⁰, and La:[Kr]4d¹⁰, and the number of valence electrons N_e is 10 for the alkaline earth metals AE, $N_e = 12$ for Zn, $N_e = 5$ for $X = \text{As}$ and P, and $N_e = 11$ for the group 3 elements G3. In this study, we use the Vienna Ab initio Simulation Package (VASP).⁴¹⁻⁴⁴ Here we set the plane-wave cutoff energy to be 500 eV, and the crystal structure is optimized until the residual Hellmann-Feynman forces become smaller than 0.01 eV/Å, and the spin-orbit coupling is not taken into account in this study.

In this study, the primitive cell is determined first by optimizing both of the lattice constants and atomic positions, where the Monkhorst-Pack (MP) $13 \times 13 \times 7$ k -point grids in the Brillouin zone are taken in the structural optimization. In the supercell calculations, the $N_1 \times N_2 \times N_3$ supercell is constructed by setting the supercell lattice vectors $\mathbf{A}_i = N_i \mathbf{a}_i$ ($i = 1, 2, 3$) with \mathbf{a}_i being the obtained i -th primitive lattice vector, and then only the atomic positions are relaxed in the

structural optimization. To obtain the formation energies in the dilute limit, the $3 \times 3 \times 2$, $3 \times 3 \times 3$, $4 \times 4 \times 2$, and $4 \times 4 \times 3$ supercells are considered for extrapolation, where gamma-centered (G) $6 \times 6 \times 3$, MP $5 \times 5 \times 3$, MP $5 \times 5 \times 3$, and G $4 \times 4 \times 3$ k -point grids are used respectively.

When each of the formation energy of the charged states in the dilute limit is evaluated from the supercell calculations, the total energies of the supercell with dopant D^q in charged state q including the point-charge correction, $\{E[D^q] + E_{1/L}^{\text{corr}}\}$, are fitted by the least squares method as a function $E_\infty + C/L^3$. Here E_∞ represents the desirable total energy in the dilute limit ($L \rightarrow \infty$), and C is a fitting parameter arising from the higher-order correction of $O(1/L^3)$.

III. RESULTS

A. Crystal and electronic structures of CaZn_2X_2 ($X = \text{As}, \text{P}$)

Before considering chemical doping, we first look at the crystal and electronic structures of CaZn_2X_2 ($X = \text{As}, \text{P}$). The crystal structure, and the lattice constants a and c , volume of the primitive cell V , and energy band gap E_g^{GGA} evaluated using GGA are shown in FIG. 1. All of the crystal structures shown in this paper are depicted by using the VESTA software.⁴⁵ Each of the evaluated energy band gaps is the direct band gap at the Γ point.

Here the obtained band gap is underestimated since GGA usually provides a smaller band gap for semiconductors than the experimental one. In fact, although the experimental band gap for CaZn_2Sb_2 is finite (~ 0.26 eV),²² the evaluated band gap disappears within GGA ($E_g^{\text{GGA}} = 0$). From now on, we do not refer to CaZn_2Sb_2 in our numerical calculations.

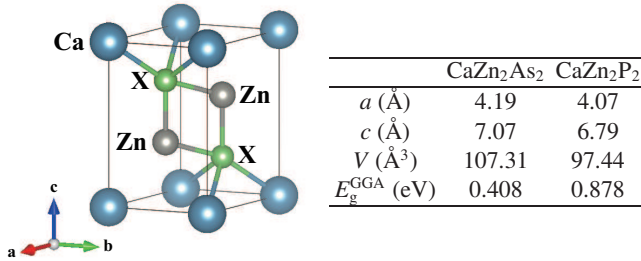


FIG. 1. (Color online) (Left) Crystal structure of CaAl_2Si_2 -type Zintl phase compound CaZn_2X_2 ($X = \text{As}, \text{P}$). (Right) Their lattice constants a and c , volume of the unit cell V , and band gap E_g^{GGA} evaluated using GGA.

In the same calculation conditions, the macroscopic static dielectric tensor $\hat{\epsilon}$ is also calculated for obtaining the point-charge correction $E_{1/L}^{\text{corr}}$. Here $\hat{\epsilon}$ is obtained from the summation over the electronic and ionic contribution, as

$$\hat{\epsilon} = \begin{pmatrix} 33.80 & 0.00 & 0.00 \\ 0.00 & 33.81 & 0.00 \\ 0.00 & 0.00 & 21.03 \end{pmatrix} \quad (4)$$

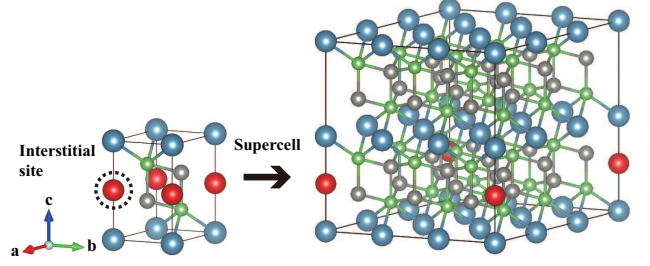


FIG. 2. (Color online) (Left) Interstitial site of CaZn_2X_2 ($X = \text{As}, \text{P}$). (Right) $3 \times 3 \times 2$ supercell with a dopant (as an example). The red ball denotes the dopant, namely, AE ($= \text{Mg}, \text{Ca}, \text{Sr}, \text{Ba}$) or $G3$ ($= \text{Sc}, \text{Y}, \text{La}$).

for CaZn_2As_2 , and

$$\hat{\epsilon} = \begin{pmatrix} 15.00 & 0.00 & 0.00 \\ 0.00 & 15.00 & 0.00 \\ 0.00 & 0.00 & 20.91 \end{pmatrix} \quad (5)$$

for CaZn_2P_2 .

B. Interstitial-site doping of AE and $G3$

We first consider the interstitial-site doping and their formation energies. Here the alkaline earth metals AE ($= \text{Mg}, \text{Ca}, \text{Sr}, \text{Ba}$) and group 3 elements $G3$ ($= \text{Sc}, \text{Y}, \text{La}$) are chosen to be a dopant since they are expected to be cations AE^{2+} and $G3^{3+}$, and hence expected to achieve n-type doping. This is an idea analogous to the one adopted for $\text{Mg}_{3+\delta}(\text{Sb}, \text{Bi}, \text{Te})_2$, where excess Mg is introduced to the interstitial site of Mg_3Sb_2 so as to realize n-type doping.^{12,13}

The interstitial sites of CaZn_2X_2 and a supercell with a dopant ($3 \times 3 \times 2$ as an example) are shown in FIG. 2. Since the formation energy of chemical doping is generally given by Eq. (1), we numerically evaluate the formation energy of the interstitial-site doping with dopant D ($= AE, G3$) in this situation,

$$E_{\text{form}} = \{E[D:\text{Ca}_N\text{Zn}_{2N}X_{2N} - qe^-] + E_{1/L}^{\text{corr}}\} - E[\text{Ca}_N\text{Zn}_{2N}X_{2N}] - E[D] + q(E_V + \Delta E_F), \quad (6)$$

where $E[D:\text{Ca}_N\text{Zn}_{2N}X_{2N} - qe^-]$ and $E[\text{Ca}_N\text{Zn}_{2N}X_{2N}]$ are the total energy of the supercell of CaZn_2X_2 with dopant D in a charged state with charge q and that of the perfect crystal $N_1 \times N_2 \times N_3$ ($= N$) supercell without any dopants, respectively. In this study, the total energy (chemical potential) of dopant D , $E[D]$, is determined to be that of the bulk crystal per atom.

E_{form} against the Fermi energy is displayed for CaZn_2As_2 and CaZn_2P_2 in FIG. 3 and FIG. 4, respectively. We calculate E_{form} for several charged states ($q = 0, +1, +2, +3, +4$), and the least E_{form} in these charged states is plotted against ΔE_F for each dopant case. The Fermi energy $\Delta E_F = E_F - E_V$ is measured from the valence band maximum E_V , so that

$\Delta E_F = 0$ is chosen to be the valence band maximum, while the conduction band minimum is located at $\Delta E_F = 0.408$ eV and 0.878 eV for CaZn_2As_2 and CaZn_2P_2 , respectively (see E_g^{GGA} in Fig. 1).

When one focuses on the conduction band minimum to see the feasibility of the n-type (electron carrier) doping, it can be observed that the formation energies of $AE = \text{Ca}, \text{Mg}$ or $G3 = \text{Sc}, \text{Y}$ are relatively small compared to the other dopants for both CaZn_2X_2 ($X = \text{As}, \text{P}$), so that these dopants are relatively favorable for n-type doping within the interstitial doping of the dopants considered here. On the other hand, it appears that spontaneous doping of these dopants may be unlikely as far as these calculation results are concerned because these formation energies are all positive. One can also see that the relative magnitude of E_{form} among the dopants is very similar between $X = \text{As}$ and P , i.e., $\text{Ca} < \text{Mg} < \text{Sr} < \text{Ba}$ and $\text{Sc} < \text{Y} < \text{La}$, and that each formation energy for CaZn_2As_2 is smaller than that for CaZn_2P_2 as a whole. Since E_{form} at the conduction band bottom is always positive, it is not clear whether interstitial-site doping can actually result in n-type doping. Nonetheless, these combinations might be possible candidates since E_{form} for CaZn_2As_2 with $AE = \text{Ca}, \text{Mg}$ or $G3 = \text{Sc}$ are relatively small.

C. G3 substitutional doping for Ca site

Next we consider the $G3$ ($= \text{Sc}, \text{Y}, \text{La}$) substitutional doping for the Ca site. As mentioned in the Introduction, element A defects tend to arise in 122 Zintl phase compounds AB_2X_2 ,^{12,13,19,28} so we assume that the introduction of dopant D compensates for the Ca vacancy. Here the group 3 elements $G3$ ($= \text{Sc}, \text{Y}, \text{La}$) are chosen to be a dopant since they are expected to be cation $G3^{3+}$ substituting Ca^{2+} , and hence result in n-type doping.

The Ca site of CaZn_2X_2 and a supercell with a dopant ($3 \times 3 \times 2$ as an example) are displayed in FIG. 5. As in the case of the interstitial-site doping, the formation energy in this situation is now evaluated numerically from Eq. (1), as

$$E_{\text{form}} = \{E[(\text{Ca}_{N-1}D)\text{Zn}_{2N}X_{2N} - qe^-] + E_{1/L}^{\text{corr}}\} + E[\text{Ca}] - E[\text{Ca}_N\text{Zn}_{2N}X_{2N}] - E[D] + q(E_V + \Delta E_F), \quad (7)$$

where $E[(\text{Ca}_{N-1}D)\text{Zn}_{2N}X_{2N} - qe^-]$ represents the supercell of CaZn_2X_2 , where Ca is substituted with the dopant D in a charged state with charge q . The charged states $q = -1, 0, +1, +2$ are considered in the present case of the substitutional doping. Similarly to the case of the interstitial doping, $E[D]$ and $E[\text{Ca}]$ are determined as the energy of the bulk crystal per atom. E_{form} against the Fermi energy is shown for CaZn_2As_2 and CaZn_2P_2 in FIG. 6 and FIG. 7, respectively.

Again focusing on the conduction band minimum, one can observe that the formation energies of $G3 = \text{La}, \text{Y}$ are relatively small compared to the other dopants. In particular, we notice that La can be substituted spontaneously for the Ca site since the formation energy is negative for CaZn_2X_2 ($X = \text{As}, \text{P}$). As in the case of interstitial doping, the relative magnitude

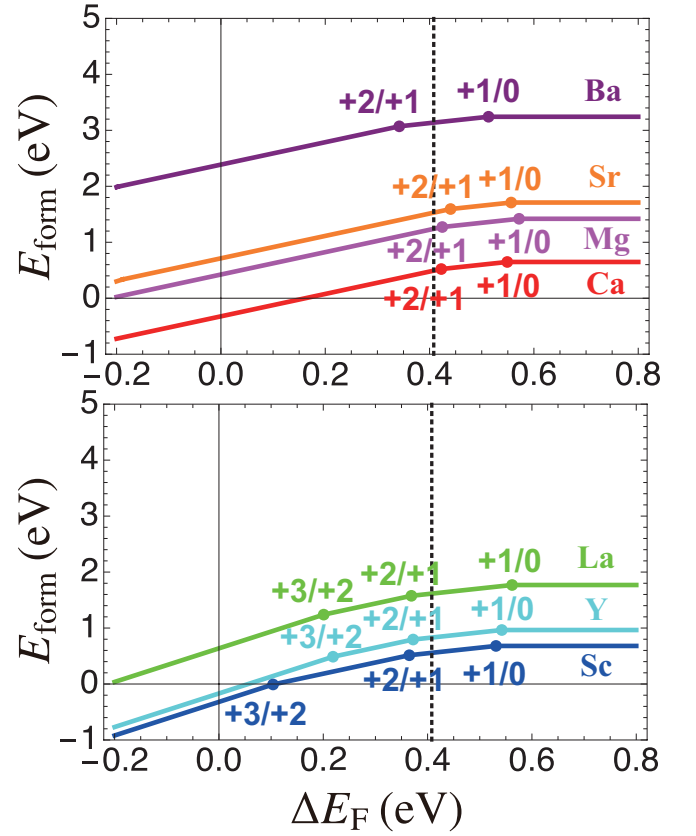


FIG. 3. (Color online) The formation energy of the interstitial-site doping E_{form} against the Fermi energy $\Delta E_F = E_F - E_V$ for CaZn_2As_2 . (Top) The alkaline earth metal AE ($= \text{Mg}, \text{Ca}, \text{Sr}, \text{Ba}$) and (Bottom) group 3 elements $G3$ ($= \text{Sc}, \text{Y}, \text{La}$) are chosen as dopant D . The least formation energy among different charged states ($q = 0, +1, +2, +3$) is plotted at each ΔE_F , where the change of the charge is indicated at each points where the slope of the line changes. The dotted line denotes the position of the conduction band minimum ($\Delta E_F = 0.408$ eV).

of E_{form} among different dopants is the same between $X = \text{As}$ and P , and also E_{form} tends to be smaller for $X = \text{As}$ than for $X = \text{P}$.

IV. DISCUSSION

In the previous sections, we have considered interstitial-site doping of alkaline earth metals and group 3 elements $G3$, and $G3$ substitutional doping for the Ca site as a possible candidate for n-type doping. Both for CaZn_2X_2 ($X = \text{As}, \text{P}$), the interstitial-site doping of $AE = \text{Ca}, \text{Mg}$ or $G3 = \text{Sc}, \text{Y}$, and $G3 = \text{La}, \text{Y}$ substitutional doping are favorable in terms of energy stability, and also, each of these formation energies for CaZn_2As_2 is small compared to that of CaZn_2P_2 . In particular, the formation energy for the La substitutional doping is the lowest among the considered cases both for CaZn_2X_2 ($X = \text{As}, \text{P}$) and is negative, so that La is expected to be substituted for the Ca site and to provide electron carriers spontaneously.

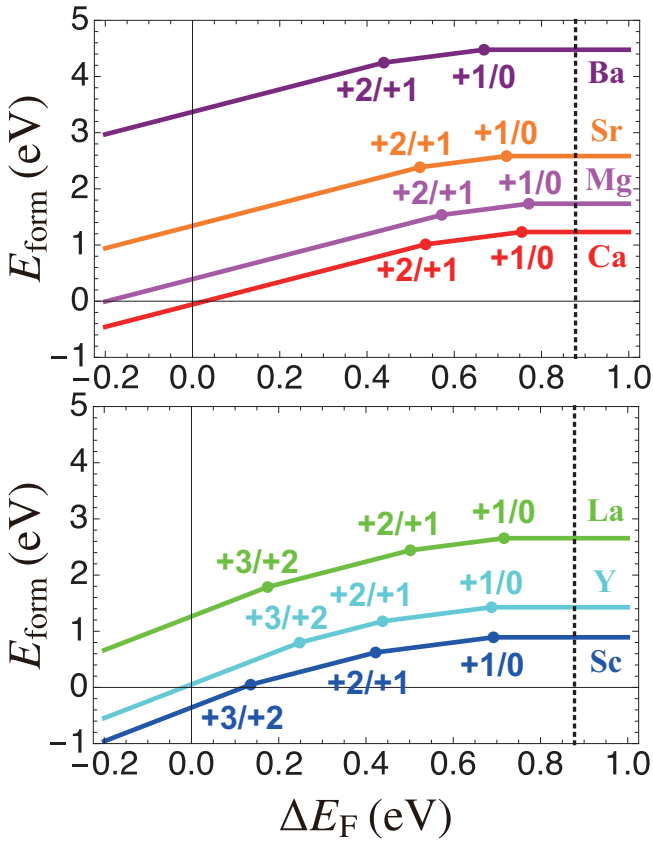


FIG. 4. (Color online) Plots similar to FIG. 3 for CaZn_2P_2 . The dotted line denotes the position of the conduction band minimum ($\Delta E_F = 0.878$ eV).

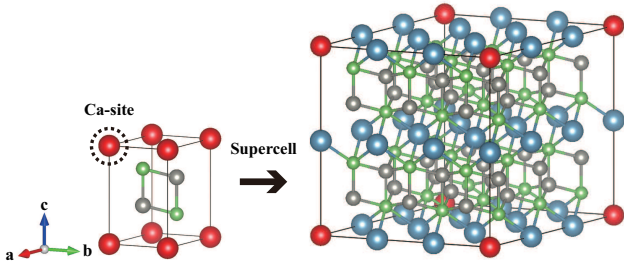


FIG. 5. (Color online) (Left) Ca site of CaZn_2X_2 ($X = \text{As}, \text{P}$). (Right) $3 \times 3 \times 2$ supercell with a dopant (as an example). The red ball denotes the dopant, namely, $G3$ ($= \text{Sc}, \text{Y}, \text{La}$).

A relevant factor to the above mentioned tendency is considered to be the ionic radius of the dopants AE and $G3$. For the interstitial-site doping, the formation energy becomes smaller with decreasing the ionic radius among AE or $G3$ ($r_{\text{Mg}^{2+}} < r_{\text{Ca}^{2+}} < r_{\text{Sr}^{2+}} < r_{\text{Ba}^{2+}}$ and $r_{\text{Sc}^{3+}} < r_{\text{Y}^{3+}} < r_{\text{La}^{3+}}$) except for Ca and Mg, where the formation energy is larger for the latter. For the $G3$ substitutional doping, the formation energy becomes smaller when the ionic radius of the dopant becomes closer to that of Ca. In fact, the ionic radius of Ca ($r_{\text{Ca}^{2+}} \sim 100$

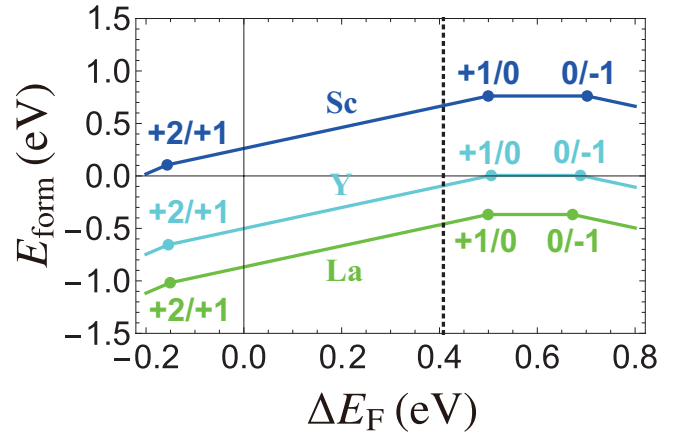


FIG. 6. (Color online) The formation energy of the $G3$ substitutional doping for the Ca site E_{form} against the Fermi energy $\Delta E_F = E_F - E_V$ for CaZn_2As_2 . The group 3 elements $G3$ ($= \text{Sc}, \text{Y}, \text{La}$) are chosen as dopant D . The dotted line denotes the position of the conduction band minimum ($\Delta E_F = 0.408$ eV).

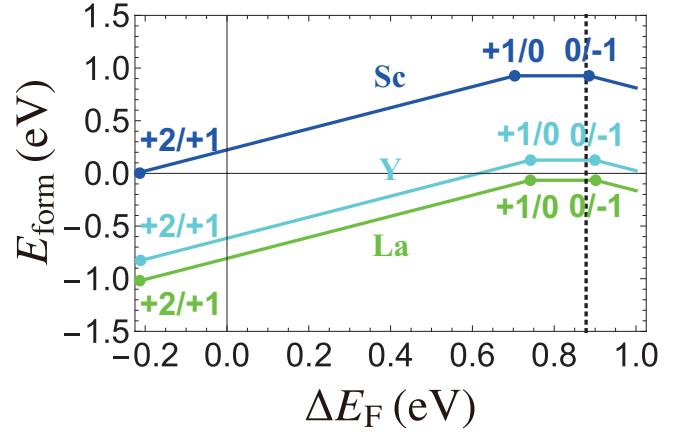


FIG. 7. (Color online) Plots similar to FIG. 6 for CaZn_2P_2 . The dotted line denotes the position of the conduction band minimum ($\Delta E_F = 0.878$ eV).

pm) is very close to that of La^{3+} ($r_{\text{La}^{3+}} \sim 103$ pm),^{46,47} and the formation energy of La substitutional doping for the Ca site is the lowest among the considered dopants.

From the viewpoint of actual experiments, possibility of n-type doping of CaZn_2Sb_2 is also of great interest, but in the present study, we focused only on $X = \text{As}$ and P . As already mentioned, the reason for this is because the band gap closes for CaZn_2Sb_2 , which is an artifact of GGA. Nonetheless, if we assume that the tendency found in the present study between $X = \text{As}$ and P also holds among $X = \text{Sb}, \text{As}$ and P , i.e., the formation energy behaves as $\text{CaZn}_2\text{Sb}_2 < \text{CaZn}_2\text{As}_2 < \text{CaZn}_2\text{P}_2$, CaZn_2Sb_2 would be more favorable for n-type doping compared to CaZn_2As_2 and CaZn_2P_2 .

In fact, since GGA generally underestimates the band gap, this would affect the formation energy, and even its sign could change. Therefore, even for CaZn_2As_2 and CaZn_2P_2 , we can-

not be completely certain about the possibility of spontaneous doping. Nevertheless, we believe that the overall systematic tendency among the dopants is grasped within the present study.

V. SUMMARY

To summarize, we explored the possibility of n-type doping of CaAl_2Si_2 -type Zintl phase compounds CaZn_2X_2 ($X = \text{As}, \text{P}$) using first-principle calculations. Among the considered possibilities, the interstitial-site doping of $AE = \text{Ca}, \text{Mg}$ or $G3 = \text{Sc}, \text{Y}$, and the $G3 = \text{La}, \text{Y}$ substitutional doping for the Ca have been found to have relatively small formation energies. In particular, the formation energy of the La substitutional doping is found to be negative for both CaZn_2As_2 and CaZn_2P_2 . This suggests that La can substitute the Ca

site spontaneously and hence provide electron carriers, as far as these calculation results are concerned. We have also found that the formation energies of the defects are smaller for CaZn_2As_2 than for CaZn_2P_2 , which suggests that n-type doping is relatively easier for the former than for the latter.

ACKNOWLEDGMENTS

We wish to thank H. Mori (RIKEN) and H. Usui (Shimane Univ.) for fruitful discussions. This work was supported by JST CREST (Grant No. JPMJCR20Q4) and JSPS KAKENHI Grant No. JP21K04866. Numerical calculations were done by the supercomputing systems at the Institute for Solid State Physics (ISSP) Supercomputer Center of the University of Tokyo and the Information Technology Center of the University of Tokyo.

- ¹ X. Zhang and L.-D. Zhao, *Journal of Materiomics* **1**, 92 (2015).
- ² S. M. Kauzlarich, S. R. Brown, and G. Jeffrey Snyder, *Dalton Transactions*, 2099 (2007).
- ³ A. I. Hochbaum, R. Chen, R. D. Delgado, W. Liang, E. C. Garnett, M. Najarian, A. Majumdar, and P. Yang, *Nature* **451**, 163 (2008).
- ⁴ A. I. Boukai, Y. Bunimovich, J. Tahir-Kheli, J.-K. Yu, W. A. Goddard III, and J. R. Heath, *Nature* **451**, 168 (2008).
- ⁵ B. Poudel, Q. Hao, Y. Ma, Y. Lan, A. Minnich, B. Yu, X. Yan, D. Wang, A. Muto, D. Vashae, and et al., *Science* **320**, 634 (2008).
- ⁶ Y. Pei, X. Shi, A. LaLonde, H. Wang, L. Chen, and G. J. Snyder, *Nature* **473**, 66 (2011).
- ⁷ K. Kuroki and R. Arita, *Journal of the Physical Society of Japan* **76**, 083707 (2007).
- ⁸ L. D. Hicks, *Physical Review B* **47**, 12727 (1993).
- ⁹ L. D. Hicks, *Physical Review B* **47**, 16631 (1993).
- ¹⁰ M. Dresselhaus, G. Chen, M. Tang, R. Yang, H. Lee, D. Wang, Z. Ren, J.-P. Fleurial, and P. Gogna, *Advanced Materials* **19**, 1043 (2007).
- ¹¹ Z. Liu, J. Mao, J. Sui, and Z. Ren, *Energy & Environmental Science* **11**, 23 (2018).
- ¹² H. Tamaki, H. K. Sato, and T. Kanno, *Advanced Materials* **28**, 10182 (2016).
- ¹³ S. Ohno, K. Imasato, S. Anand, H. Tamaki, S. D. Kang, P. Gorai, H. K. Sato, E. S. Toberer, T. Kanno, and G. J. Snyder, *Joule* **2**, 141 (2018).
- ¹⁴ X. Shi, T. Zhao, X. Zhang, C. Sun, Z. Chen, S. Lin, W. Li, H. Gu, and Y. Pei, *Advanced Materials* **31**, 1903387 (2019).
- ¹⁵ J. Shuai, J. Mao, S. Song, Q. Zhang, G. Chen, and Z. Ren, *Materials Today Physics* **1**, 74 (2017).
- ¹⁶ S. R. Brown, S. M. Kauzlarich, F. Gascoin, and G. J. Snyder, *Chemistry of Materials* **18**, 1873 (2006).
- ¹⁷ S. Ohno, U. Aydemir, M. Amsler, J.-H. Pöhls, S. Chanakian, A. Zevalkink, M. A. White, S. K. Bux, C. Wolverton, and G. J. Snyder, *Advanced Functional Materials* **27**, 1606361 (2017).
- ¹⁸ X.-J. Wang, M.-B. Tang, H.-H. Chen, X.-X. Yang, J.-T. Zhao, U. Burkhardt, and Y. Grin, *Applied Physics Letters* **94**, 092106 (2009).
- ¹⁹ W. Peng, S. Chanakian, and A. Zevalkink, *Inorganic Chemistry Frontiers* **5**, 1744 (2018).
- ²⁰ J. Zhang, L. Song, S. H. Pedersen, H. Yin, L. T. Hung, and B. B. Iversen, *Nature Communications* **8** (2017), 10.1038/ncomms13901.
- ²¹ J. Zhang and B. B. Iversen, *Journal of Applied Physics* **126**, 085104 (2019).
- ²² E. S. Toberer, A. F. May, B. C. Melot, E. Flage-Larsen, and G. J. Snyder, *Dalton Trans.* **39**, 1046 (2010).
- ²³ H. Usui and K. Kuroki, *Journal of the Physical Society of Japan* **89**, 124707 (2020).
- ²⁴ F. Gascoin, S. Ottensmahn, D. Stark, S. Haïle, and G. Snyder, *Advanced Functional Materials* **15**, 1860 (2005).
- ²⁵ A. F. May, M. A. McGuire, J. Ma, O. Delaire, A. Huq, and R. Custelcean, *Journal of Applied Physics* **111**, 033708 (2012).
- ²⁶ K. Kihou, H. Nishiate, A. Yamamoto, and C. H. Lee, *Inorganic Chemistry* **56**, 3709 (2017).
- ²⁷ D. J. Singh, *Journal of Materials Chemistry A* **5**, 17088 (2017).
- ²⁸ G. S. Pomrehn, A. Zevalkink, W. G. Zeier, A. van de Walle, and G. J. Snyder, *Angewandte Chemie International Edition* **53**, 3422 (2014).
- ²⁹ S. B. Zhang and J. E. Northrup, *Phys. Rev. Lett.* **67**, 2339 (1991).
- ³⁰ H.-P. Komsa, T. T. Rantala, and A. Pasquarello, *Phys. Rev. B* **86**, 045112 (2012).
- ³¹ M. Leslie and N. J. Gillan, *Journal of Physics C: Solid State Physics* **18**, 973 (1985).
- ³² G. Makov and M. C. Payne, *Phys. Rev. B* **51**, 4014 (1995).
- ³³ L. M. Fraser, W. M. C. Foulkes, G. Rajagopal, R. J. Needs, S. D. Kenny, and A. J. Williamson, *Phys. Rev. B* **53**, 1814 (1996).
- ³⁴ I. Dabo, B. Kozinsky, N. E. Singh-Miller, and N. Marzari, *Phys. Rev. B* **77**, 115139 (2008).
- ³⁵ J. M. Ziman, *Principles of the Theory of Solids*, 2nd ed. (Cambridge University Press, 1972).
- ³⁶ R. Rurali and X. Cartoixa, *Nano Letters* **9**, 975 (2009).
- ³⁷ Y. Kumagai and F. Oba, *Phys. Rev. B* **89**, 195205 (2014).
- ³⁸ J. P. Perdew, K. Burke, and M. Ernzerhof, *Phys. Rev. Lett.* **77**, 3865 (1996).
- ³⁹ P. E. Blöchl, *Phys. Rev. B* **50**, 17953 (1994).
- ⁴⁰ G. Kresse and D. Joubert, *Phys. Rev. B* **59**, 1758 (1999).
- ⁴¹ G. Kresse and J. Hafner, *Phys. Rev. B* **47**, 558 (1993).
- ⁴² G. Kresse and J. Hafner, *Phys. Rev. B* **49**, 14251 (1994).
- ⁴³ G. Kresse and J. Furthmüller, *Computational Materials Science* **6**, 15 (1996).
- ⁴⁴ G. Kresse and J. Furthmüller, *Phys. Rev. B* **54**, 11169 (1996).
- ⁴⁵ K. Momma and F. Izumi, *Journal of Applied Crystallography* **44**, 1272 (2011).

- ⁴⁶ R. D. Shannon and C. T. Prewitt, Acta Crystallographica Section B **25**, 925 (1969).
- ⁴⁷ R. D. Shannon, Acta Crystallographica Section A **32**, 751 (1976).